Phase diagram of quark-antiquark and diquark condensates in the 3-dimensional Gross-Neveu model with the 4-component spinor representation

Hiroaki Kohyama*

Department of Physics, Osaka City University, Sumiyoshi-ku, Osaka 558-8585, Japan

(Received 14 March 2008; published 28 July 2008)

We construct the phase diagram of the quark-antiquark and diquark condensates at finite temperature and density in the $2+1$ dimensional (3D) two flavor massless Gross-Neveu (GN) model with the 4-component quarks. In contrast to the case of the 2-component quarks, there appears the coexisting phase of the quark-antiquark and diquark condensates. This is the crucial difference between the 2-component and 4-component quark cases in the 3D GN model. The coexisting phase is also seen in the 4D Nambu Jona-Lasinio model. Then we see that the 3D GN model with the 4-component quarks bears closer resemblance to the 4D Nambu Jona-Lasinio model.

DOI: 10.1103/PhysRevD.78.014021 PACS numbers: 12.38.Aw, 12.38.Lg, 11.15.Pg, 11.10.Wx

I. INTRODUCTION

Investigating the phase structure of quantum chromodynamics (QCD) has stirred a lot of interest of theorists to understand the field of strong interaction physics. QCD is an asymptotically free theory and the interactions between quarks and gluons become weak at high energy [1]. Then, at high temperature and/or density, the quarks and gluons constitute a rather weakly interacting system, which is called the quark-gluon plasma. On the other hand, at low temperature and density, quarks and gluons are confined into hadrons and cannot be observed as free particles. Furthermore, it is widely believed that the various states are realized at low temperature and moderate baryon density.

The study of QCD at low temperature and finite baryon density is a traditional issue in nuclear physics. The behavior of the cold, dense quark matter is important for astrophysics to understand the structure of compact stars and condition near the core of collapsing stars. In the case of such high baryon density, the system is expected to be a color superconductor. The color superconductivity is the state in which the quarks near the Fermi surface become correlated to form quark-quark (diquark) Cooper pairs [2]. Since it was revealed that the related gaps in the fermion spectrum could be of the order 100 MeV [3], the color superconducting states have been considered as the important phases in the QCD phase diagram. For review articles on the color superconductivity, see e.g. [4].

One of the simple theories to treat the above-mentioned subject is the Nambu Jona-Lasinio (NJL) model, which is a low energy effective field theory of QCD [5]. The NJL model successfully describes the QCD phase structure, and a variety of works has been devoted to the study on the basis of the NJL model. (For reviews, see, e.g. [6,7].) In particular, through analysis on the competition between quark-antiquark ($q\bar{q}$) and diquark (qq) condensates in the NJL model, it has been found that there appears the coexisting phase of the $q\bar{q}$ and qq condensates (see [7]).

The study of the phase structure of the NJL model in lower dimensions (D) is also an interesting issue since the models usually become simpler in lower dimensions [8]. Indeed, the Gross-Neveu (GN) model [9], which is the counterpart of the NJL model in 2D and 3D, becomes renormalizable. Since the GN model shares many properties with QCD, it has been regarded as an important model and there have been a great deal of works on it [10–15]. The phase diagram of the $q\bar{q}$ condensate within the original 2D GN model was derived in [12], and the phase diagram in the 3D GN model was obtained in [13]. Recently, by using the mean-field approximation, the phase structure of the $q\bar{q}$ and qq condensates was studied within the 3D GN model [14,15].

It is worth mentioning that, in 3D at finite temperature, Hohenberg proved that the qq condensate does not happen by evaluating the fluctuations of the order parameter in superfluids and superconductors [16]. He used the Bogoliubov inequality to show the assumption of a broken symmetry in Bose or Fermi liquids leads to a contradiction. Mermin and Wagner also proved that, at finite temperature, the 3D isotropic Heisenberg model with finite-range exchange interaction can be neither ferromagnetic nor antiferromagnetic [17]. Furthermore, Coleman showed that the Goldstone phenomenon [18] cannot occur in 3D [19]. These results are called the Mermin-Wagner-Coleman theorem and it prohibits the spontaneous breaking of a continuous symmetry in 3D at finite temperature. However, I believe, it is worth studying the competition between the $q\bar{q}$ and qq condensates through evaluating the renormalized effective potential from the phenomenological point of view. In fact, the $q\bar{q}$ and qq condensates could be formed in the 3D GN model as shown in [14,15].

In [14,15], the quarks are assigned to the lowest nontrivial (2-dimensional) representation of the $O(2,1)$ group which we refer to as the 2-component (2c) quarks. The resultant phase diagrams show that there does not appear

*kohyama@sci.osaka-cu.ac.jp

the region where the $q\bar{q}$ and qq condensates coexist, which is in sharp contrast to the 4D NJL case. This difference may stem from the difference in form of the qq condensate term in the Lagrangian between them. In the 2c quark case in 3D, the qq condensate term in the Lagrangian does not include the γ^5 matrix, which leads to the above-mentioned difference. However, as discussed in [20], the γ^5 enters in the case of the 4c quarks in 3D. In this sense, the 3D GN model with the 4c quarks is expected to bear closer resemblance to the 4D NJL model. Actually, in vacuum (zero temperature and chemical potential) theory, the coexisting phase of the $q\bar{q}$ and qq condensates has been found in the 3D GN model with the 4c quarks [21]. The relation between the 2c and 4c quark cases is discussed in [10].

In this paper, we study the $q\bar{q}$ and qq condensates at finite temperature and density in the 3D two flavor massless GN model with the 4c quarks. We construct the phase diagrams, and discuss the similarities and differences among the models, the 3D GN model with the 4c quarks, the 3D GN model with the 2c quarks, and the 4D NJL model.

The paper is organized as follows: In Sec. II we introduce the Lagrangian density in the 3D GN model with the 4c quarks and apply the mean-field approximation. In Sec. III the derivation of the thermodynamic potential is given. Then, in Sec. IV, we show the numerical results for the $q\bar{q}$ and qq condensates at zero and finite temperature. In Sec. V, the phase diagrams of the $q\bar{q}$ and qq condensates are obtained. Section VI is devoted to concluding remarks.

II. 3D GROSS-NEVEU MODEL

A. Preliminary

We start with the following Lagrangian density which includes the diquark interaction term,

$$\mathcal{L} = \bar{q}i\not{\partial}q + G_S[(\bar{q}q)^2 + (\bar{q}i\vec{\tau}\gamma^5 q)^2] + G_D(q^{\mathrm{T}}\mathcal{O}q)^2. \tag{1}$$

Here $q \equiv q_{\alpha k}$ has two flavors $\alpha = u, d$ and three colors $k = r$ (*red*), g (*green*), b (*blue*) degrees of freedom. $\vec{\tau} = (\tau_1, \tau_2, \tau_3)$ are the Pauli matrices in flavor space and $\mathcal{O}$ denotes an operator acting in Dirac, flavor, and color spaces. G_S and G_D are the coupling constants of the $q\bar{q}$ and qq interactions.

The form of the diquark interaction is determined by the following consideration: First, the Pauli principle requires the matrix $\mathcal{O}$ to be totally antisymmetric operators, since

$$q^{\mathrm{T}}\mathcal{O}q = \mathcal{O}_{ij}q_iq_j = -\mathcal{O}_{ij}q_jq_i = -q^{\mathrm{T}}\mathcal{O}^{\mathrm{T}}q. \tag{2}$$

Concerning the operator in color space, we choose the color antitriplet matrices $(\lambda_2, \lambda_5, \lambda_7)$ because the attractive interaction becomes the important contribution near the Fermi surface [3]. The renormalization group arguments [22] indicate that the operator in spinor space is also antisymmetric. This means that the operator in flavor space has to be antisymmetric. Then we restrict the form of the Lagrangian equation (1) as

$$\mathcal{L} = \bar{q}i\not{\partial}q + G_S[(\bar{q}q)^2 + (\bar{q}i\vec{\tau}\gamma^5 q)^2] + G_D\sum_{a=2,5,7}(\bar{q}i\tau_2\lambda_a\gamma^5 q^C)(\bar{q}^C i\tau_2\lambda_a\gamma^5 q), \tag{3}$$

where τ_2 is the antisymmetric matrix in flavor space and C expresses the charge conjugation. The charge conjugated fields are given by $q^C = C\bar{q}^{\mathrm{T}}$, $\bar{q}^C = q^{\mathrm{T}}C$, with the charge conjugation matrix C. Without loss of generality, one can choose a color direction for diquark condensate to *blue*, which is equivalent to leaving λ_2 in Eq. (3). Then the Lagrangian becomes

$$\mathcal{L} = \bar{q}i\not{\partial}q + G_S[(\bar{q}q)^2 + (\bar{q}i\vec{\tau}\gamma^5 q)^2] + G_D(\bar{q}i\tau_2\lambda_2\gamma^5 q^C)(\bar{q}^C i\tau_2\lambda_2\gamma^5 q). \tag{4}$$

As done in [7,14,15], we focus on the competition between two condensates $\langle\bar{q}q\rangle$ and $\langle\bar{q}^C i\tau_2\lambda_2\gamma^5 q\rangle$, and drop the term $(\bar{q}i\vec{\tau}\gamma^5 q)^2$.

B. The model

Observing the above speculation, we employ the following Lagrangian density of the 3D two flavor massless Gross-Neveu model with the diquark interaction,

$$\mathcal{L} = \bar{q}i\not{\partial}q + G_S(\bar{q}q)^2 + G_D(\bar{q}i\tau_2\lambda_2\gamma^5 q^C)(\bar{q}^C i\tau_2\lambda_2\gamma^5 q). \tag{5}$$

In the 4-component spinor representation in 3D, the Dirac matrices are the 4×4 matrices and we use the same form as used in [20],

$$\gamma^0 = \begin{pmatrix}\tau_3 & 0\\ 0 & -\tau_3\end{pmatrix},\quad \gamma^1 = \begin{pmatrix}i\tau_1 & 0\\ 0 & -i\tau_1\end{pmatrix},\quad \gamma^2 = \begin{pmatrix}i\tau_2 & 0\\ 0 & -i\tau_2\end{pmatrix},\quad \gamma^5 = i\begin{pmatrix}0 & 1\\ -1 & 0\end{pmatrix}. \tag{6}$$

The Lagrangian in Eq. (5) is invariant under the following transformations:

(1) Parity $\mathcal{P}$: $q(t, x, y) \to \gamma^5\gamma^1 q(t, -x, y)$
(2) Time reversal $\mathcal{T}$: $q(t, \vec{x}) \to i\gamma^2\gamma^5 q(-t, \vec{x})$
(3) Charge conjugation $\mathcal{C}$: $q^C \to \gamma^2\bar{q}^{\mathrm{T}}$, $\bar{q}^C \to q^{\mathrm{T}}\gamma^2$
(4) Discrete chiral symmetry $\mathcal{X}_D$: $q \to \gamma^5 q$.

It should be noted that the inversion of both axes $(x, y) \to (-x, -y)$ could be achieved by the rotation. Then we considered the parity transformation $(x, y) \to (-x, y)$ as in [20]. The symmetry properties of the 4c quarks and the relation between 4c and 2c quarks are discussed in the papers [10,20] in more detail.

With the aim to study the system near the Fermi surface, we introduce the mean-field approximation

$$\sigma = -2G_S\langle\bar{q}q\rangle, \qquad \Delta = 2G_D\langle\bar{q}^C i\tau_2\lambda_2\gamma^5 q\rangle. \tag{7}$$

Here σ and Δ are the order parameters for the $q\bar{q}$ and qq condensates, respectively. Within the mean-field approxi-

mation, the Lagrangian can be written by

$$\tilde{\mathcal{L}} = \bar{q}(i\partial - \sigma)q + \frac{1}{2}\Delta^*(\bar{q}^C i\tau_2\lambda_2\gamma^5 q) + \frac{1}{2}\Delta(\bar{q} i\tau_2\lambda_2\gamma^5 q^C) - \frac{\sigma^2}{4G_S} - \frac{|\Delta|^2}{4G_D}. \quad (8)$$

The nonzero expectation value σ and Δ indicate that the chiral symmetry and the color symmetry are spontaneously broken.

III. THE THERMODYNAMIC POTENTIAL

A. Derivation of the thermodynamic potential

The partition function of the ground canonical ensemble is calculated by using the standard method,

$$\mathcal{Z} = N' \int [d\bar{q}][dq] \exp\left\{\int_0^\beta d\tau \int d^2\mathbf{x}(\tilde{\mathcal{L}} + \mu\bar{q}\gamma_0 q)\right\}, \quad (9)$$

where $\beta = 1/T$ is the inverse temperature and μ is the quark chemical potential. Introducing the Nambu-Gorkov basis [23]

$$\Psi = \begin{pmatrix} q \\ q^C \end{pmatrix} \quad \text{and} \quad \bar{\Psi} = (\bar{q}\bar{q}^C), \quad (10)$$

we have

$$\mathcal{Z} = N' \exp\left\{-\int_0^\beta d\tau \int d^2\mathbf{x}\left(\frac{\sigma^2}{4G_S} + \frac{|\Delta|^2}{4G_D}\right)\right\} \times \int [d\Psi] \exp\left\{\frac{1}{2}\sum_{n,\mathbf{p}} \bar{\Psi}(\beta G^{-1})\Psi\right\}. \quad (11)$$

The matrix G^{-1} is defined by

$$G^{-1} = \begin{pmatrix} (\not{p} - \sigma + \mu\gamma^0)\mathbf{1}_f\mathbf{1}_c & i\tau_2\lambda_2\gamma^5\Delta \\ i\tau_2\lambda_2\gamma^5\Delta^* & (\not{p} - \sigma - \mu\gamma^0)\mathbf{1}_f\mathbf{1}_c \end{pmatrix}, \quad (12)$$

where $\mathbf{1}_f$ and $\mathbf{1}_c$ are the unit matrix in flavor and color spaces, respectively.

Then the thermodynamic potential $\Omega = -\ln\mathcal{Z}/\beta V$ becomes

$$\Omega(\sigma, |\Delta|) = \frac{\sigma^2}{4G_S} + \frac{|\Delta|^2}{4G_D} - \frac{1}{\beta V}\ln\int [d\Psi] \times \exp\left[\frac{1}{2}\sum_{n,p} \bar{\Psi}(\beta G^{-1})\Psi\right], \quad (13)$$

where V is the volume of the thermal system. By applying the formula

$$\int [d\Psi] \exp\left[\frac{1}{2}\sum_{n,p} \bar{\Psi}(\beta G^{-1})\Psi\right] = \det{}^{1/2}(\beta G^{-1}), \quad (14)$$

we obtain

$$\Omega(\sigma, |\Delta|) = \frac{\sigma^2}{4G_S} + \frac{|\Delta|^2}{4G_D} - \frac{1}{\beta V}\ln\det{}^{1/2}(\beta G^{-1}). \quad (15)$$

After some manipulations [7], the determinant becomes

$$\det{}^{1/2}(G^{-1}) = [p_0^2 - E_\Delta^{+2}]^4[p_0^2 - E_\Delta^{-2}]^4[p_0^2 - E^{+2}]^2 \times [p_0^2 - E^{-2}]^2, \quad (16)$$

where $p_0 = i(2n+1)\pi T$, $(n = \cdots, -2, -1, 0, 1, 2, \cdots)$ and

$$E_\Delta^{\pm 2} \equiv (E \pm \mu)^2 + |\Delta|^2, \qquad E^\pm \equiv E \pm \mu, \qquad E \equiv \sqrt{\vec{p}^2 + \sigma^2}, \qquad \vec{p}^2 = p_1^2 + p_2^2. \quad (17)$$

Thus, we have

$$\Omega(\sigma, |\Delta|) = \frac{\sigma^2}{4G_S} + \frac{|\Delta|^2}{4G_D} - 2T\sum_{\pm}\sum_n \int \frac{d^2p}{(2\pi)^2} \times [\ln[\beta^2(p_0^2 - E^{\pm 2})] + 2\ln[\beta^2(p_0^2 - E_\Delta^{\pm 2})]]. \quad (18)$$

One can carry out the frequency summation by following the standard procedure [24]

$$\sum_n \ln[\beta^2(p_0^2 - E^2)] = \beta[E + 2T\ln(1 + e^{-\beta E})]. \quad (19)$$

Then we finally obtain the thermodynamic potential

$$\Omega(\sigma, |\Delta|) = \Omega_0(\sigma, |\Delta|) + \Omega_T(\sigma, |\Delta|), \quad (20)$$

$$\Omega_0(\sigma, |\Delta|) = \frac{\sigma^2}{4G_S} + \frac{|\Delta|^2}{4G_D} - 4\int \frac{d^2p}{(2\pi)^2}[E + E_\Delta^+ + E_\Delta^-], \quad (21)$$

$$\Omega_T(\sigma, |\Delta|) = -4T\sum_{\pm}\int \frac{d^2p}{(2\pi)^2} \times [\ln(1 + e^{-\beta E^\pm}) + 2\ln(1 + e^{-\beta E_\Delta^\pm})]. \quad (22)$$

Ω_0 is the T independent contribution and Ω_T is the T dependent part. Ω_0 includes ultraviolet divergent, while Ω_T is finite.

B. Renormalized thermodynamic potential

To eliminate the divergent contribution in Ω_0, we carry out the renormalization through introducing the counter Lagrangian density [14], which is of the form $\mathcal{L}_C = -Z_S\sigma^2/2 - Z_D|\Delta|^2$. In the present case, the renormalization factors Z_S and Z_D are given by

$$Z_S = \frac{12}{\pi}\Lambda - \frac{3}{2}\alpha, \quad (23)$$

$$Z_D = \frac{4}{\pi}\Lambda - \frac{1}{2}\alpha. \quad (24)$$

Here Λ is the 3D momentum cutoff and α is an arbitrary renormalization scale.

Then, by introducing the following parameters:

$$\sigma_0 \equiv -\frac{\pi}{3}\left(\frac{1}{4G_S} - \frac{3}{4}\alpha\right), \tag{25}$$

$$\Delta_0 \equiv -\frac{\pi}{2}\left(\frac{1}{4G_D} - \frac{1}{2}\alpha\right), \tag{26}$$

we have the renormalized thermodynamic potential

$$\Omega_r(\sigma, |\Delta|) = \Omega_{0r}(\sigma, |\Delta|) + \Omega_T(\sigma, |\Delta|), \tag{27}$$

$$\begin{aligned}\Omega_{0r}(\sigma, |\Delta|) = &-\frac{3\sigma_0}{\pi}\sigma^2 - \frac{2\Delta_0}{\pi}|\Delta|^2 + \frac{2}{3\pi}\sigma^3 \\ &+ \frac{1}{3\pi}\sum_{\pm}[(2\sigma^2 + 2|\Delta|^2 - \mu^2 \pm \mu\sigma) \\ &\times \sqrt{\sigma^2 + |\Delta|^2 + \mu^2 \pm 2\mu\sigma} \\ &\mp 3\mu|\Delta|^2 \\ &\times \ln\{\sigma \pm \mu + \sqrt{\sigma^2 + |\Delta|^2 + \mu^2 \pm 2\mu\sigma}\}].\end{aligned} \tag{28}$$

σ_0 (Δ_0) is the $q\bar{q}$ (qq) condensate at $T = 0$ and $\mu = 0$ in the model when the qq ($q\bar{q}$) condensate is absent. It should be noted that the thermodynamic potential has two free parameters σ_0 and Δ_0. As in [14], we take σ_0 to be the scale of the theory ($\sigma_0 \geq 0$). Then, after fixing σ_0, there remains one free parameter Δ_0 and we study the various values for the ratio Δ_0/σ_0.

IV. QUARK-ANTIQUARK AND DIQUARK CONDENSATES

In this section, we show the numerical result of the $q\bar{q}$ and qq condensates through analyzing the thermodynamic potential, Eq. (27). The realized condensates are obtained by finding the minimum of the thermodynamic potential with respect to σ and Δ.

Figure 1 displays the results of the two condensates against μ at $T = 0$. From the panel (a) ($\Delta_0/\sigma_0 = -6$), we see that the $q\bar{q}$ condensate exists for small μ and it disappears when μ becomes large. This clearly shows the phenomena of the phase transition, and the transition chemical potential is $\mu = 1.0\sigma_0$. There does not occur the qq condensate for whole μ. However, for $\Delta_0/\sigma_0 = -1$, the qq condensate appears at $\mu = 1.0\sigma_0$, the value where the $q\bar{q}$ condensate disappears. Similar results are

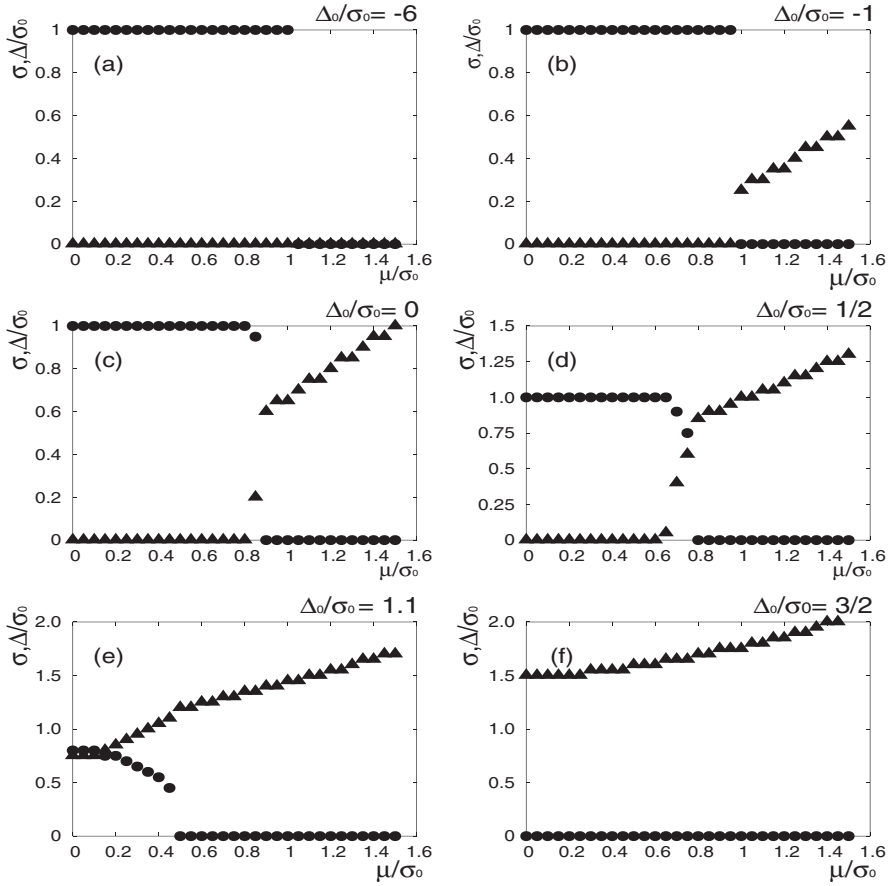

FIG. 1. σ (circles) and Δ (triangles) as a function of chemical potential μ at $T = 0$.

obtained in the cases $\Delta_0/\sigma_0 = 0, 1/2$. At some chemical potential, the $q\bar{q}$ condensate falls and the qq condensate arises. The transition chemical potentials are $\mu = 0.9\sigma_0$ and $0.8\sigma_0$ for $\Delta_0/\sigma_0 = 0$ and $1/2$, respectively. Thus the transition chemical potential becomes smaller with increasing the ratio Δ_0/σ_0, and the value of the qq condensate Δ enlarges. For $\Delta_0/\sigma_0 = 1.1$, the qq condensate at $\mu = 0$ has the close value with the $q\bar{q}$ condensate, and it eventually exceeds the $q\bar{q}$ condensate for $\Delta_0/\sigma_0 = 3/2$. Note that the $q\bar{q}$ condensate does not exist for $\Delta_0/\sigma_0 = 3/2$ and there appears only the qq condensate. Thus we see that the behaviors of the $q\bar{q}$ and qq condensates are sensitive to the value of the ratio Δ_0/σ_0.

The results of the condensates at finite temperature are shown in Fig. 2. In the panel (a) ($\Delta_0/\sigma_0 = 0$, $\mu = 0$), we see that the $q\bar{q}$ condensate occurs at $T = 0$ and it decreases when T becomes larger. The transition temperature in this case is $T = 0.65\sigma_0$. The panel (b) ($\Delta_0/\sigma_0 = 0$, $\mu = 1.0\sigma_0$) shows that the qq condensate is $0.65\sigma_0$ at $T = 0$ and it disappears at $T = 0.35\sigma_0$. Thus we see that the $q\bar{q}$ and qq condensates decrease as the temperature increases. This is also the case for $\Delta_0/\sigma_0 = 1.1$, which is shown in the panels (c) and (d). We have analyzed the cases for other values of Δ_0/σ_0, and found that the behavior of the two condensates do not change qualitatively.

It should be noted that, in Fig. 1 ($T = 0$ case), the $q\bar{q}$ condensate disappears discontinuously. This is the signal of the first-order phase transition. On the other hand, the $q\bar{q}$ condensate disappears continuously in Fig. 2(a) ($\mu = 0$ case), which indicates the second-order phase transition. This means that the critical point from the first-order phase transition to the second-order one appears at some point in the phase diagram, which we will discuss in more detail in the next section.

V. THE PHASE DIAGRAM

On the basis of the results obtained in the previous section, we construct the phase diagram. Figure 3 displays the phase structure of the $q\bar{q}$ and qq condensates for the cases $\Delta_0/\sigma_0 = -1, 0, 1/2, 1.1$.

From the panel (a), we see that the $q\bar{q}$ condensate phase is realized at low T and μ, and the qq condensate phase occurs at low T and high μ. At high T and μ, there does not exist a condensate, namely, the system is in the normal phase. The similar structure is seen in the panel (b): $q\bar{q}$ phase at low T and μ, qq phase at low T and high μ. However, in the case of $\Delta_0/\sigma_0 = 0$, we see that the coexisting phase of the $q\bar{q}$ and qq condensates appears at low T and intermediate μ. We refer to this phase as the "double broken" (DB) phase. Thus, the system is characterized by the following phases:

Q: $q\bar{q}$ condensate phase ($\sigma \neq 0$, $\Delta = 0$)
D: qq condensate phase ($\sigma = 0$, $\Delta \neq 0$)
DB: Double broken phase ($\sigma \neq 0$, $\Delta \neq 0$)
N: Normal phase ($\sigma = 0$, $\Delta = 0$)

All of these phases appear in the case of $\Delta_0/\sigma_0 = 1/2$ [panel (c)]. However the Q phase does not appear for $\Delta_0/\sigma_0 = 1.1$ and only the D phase and DB phase appear. Thus, as the ratio Δ_0/σ_0 increases, the Q condensate phase shrinks toward the μ axis and the region of the D phase and DB phase becomes larger.

The points (μ_c, T_c) in the panels (a), (b), and (c) indicate the critical points from the first-order phase transition to

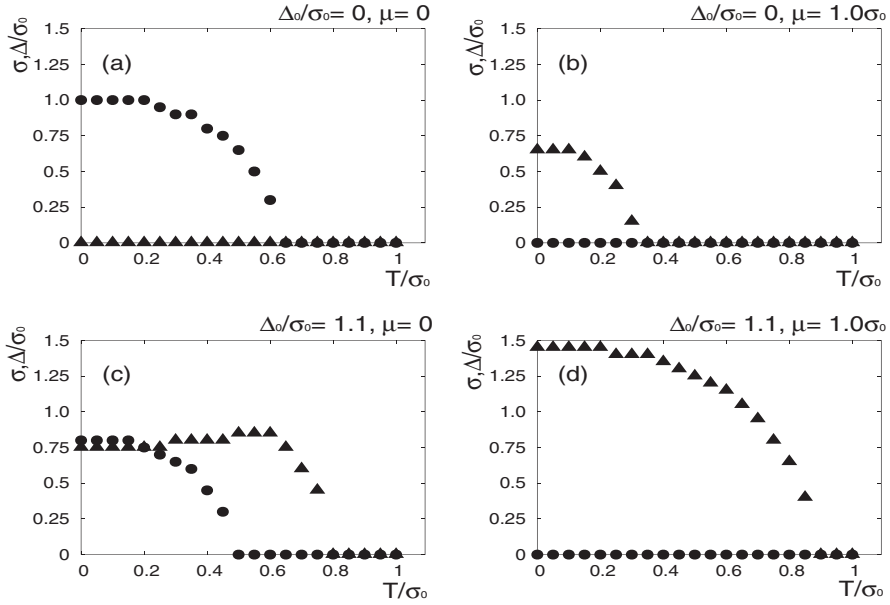

FIG. 2. The two gaps σ (circles) and Δ (triangles) against T.

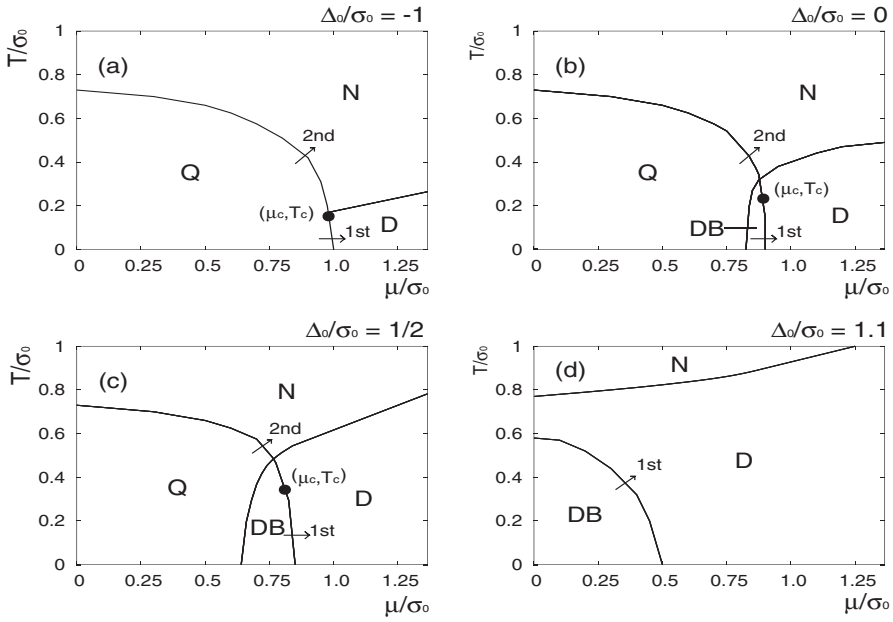

FIG. 3. The phase diagrams.

the second-order one. The phase transition below the critical temperature T_c is of the first order and above T_c is of the second order. We notice that the value of T_c increases when Δ_0/σ_0 becomes larger, while μ_c decreases with increasing Δ_0/σ_0. Then the critical point moves upward along the transition line, and the region of the first-order phase transition expands. The other phase transitions, namely, the transitions Q → DB, Q → N, and D → N, are of the second order.

VI. CONCLUDING REMARKS

Through studying the $q\bar{q}$ and qq condensates at finite temperature and chemical potential, we have obtained the phase diagrams in the 3D GN model with the 4c quarks.

We have shown that the $q\bar{q}$ condensate (Q) phase is realized at low T and μ, the double broken (DB) phase at low T and intermediate μ, and the qq condensate (D) phase at low T and high μ (see Fig. 3(b) and 3(c)). This feature bears resemblance to the case of the 4D NJL model. It is difficult to make a direct comparison between the present model and the 4D NJL model because the free parameter in the NJL model is the "direct ratio" of the coupling constants G_D/G_S, while the free parameter of the present model is the ratio Δ_0/σ_0 which is not G_D/G_S. However, the parameter Δ_0 is related to G_D through Eq. (26), and Δ_0 becomes larger as G_D increases. Then the ratio Δ_0/σ_0 increases as the qq coupling constant G_D increases. This means that, as G_D/G_S increases, the region of the Q phase shrinks, and the regions of the D phase and the DB phase expand. Then, the behavior of the phase diagrams shows the close similarity to the case of the 4D NJL model.

We are now in the position to make the comparison with the 3D GN model with the 2c quarks. Comparing with the phase diagrams in the 2c quark case obtained in [14], we see a rather similar structure: The Q phase at low T and μ, and the D phase at low T and high μ. However, there is one crucial difference. There does not appear the DB phase in the 2c quark case, while in the present 4c quark case, the DB phase does appear. The latter fact is in accord with the expectation mentioned in the introduction.

The critical points between the first-order and second-order transition are located on the Q → D phase transition line in Fig. 3(a) and on the DB → D transition line in Fig. 3 (b) and 3(c). In the model without qq condensate, the $q\bar{q}$ phase transition at zero temperature is of the first order and the transition at finite temperature is of the second order. This means that T_c is negligibly small in the model without the qq condensate, while in the present model, T_c is finite, which is the reflection of the existence of the qq condensate. It is also worth comparing the present model with the model with the 2c quarks, where the coexisting phase is absent. The phase transition Q → D is always of the first order and the critical points are seen on the line Q → N [14]. This may come from the fact that the existence of the qq condensate expels the $q\bar{q}$ condensate. On the other hand, in the present 4c quark case, the $q\bar{q}$ and qq condensates can coexist and the Q → D and DB → D transitions can be of second order.

Finally, it is worth reemphasizing that the significant qualitative difference is that there exists the $q\bar{q}$ and qq

coexisting phase in the present model, which is not seen in the 2c quark case. Then, when compared to the case of the 3D GN model with the 2c quarks, the phase structures of the present 4c quark case bear closer resemblance to the 4D NJL model.

ACKNOWLEDGMENTS

I would like to express my sincere gratitude to A. Niegawa for useful discussions and reading of the manuscript. The valuable discussions with M. Inui and T. Inagaki are also gratefully acknowledged.

[1] D. J. Gross and F. Wilczek, Phys. Rev. Lett. **30**, 1343 (1973); H. D. Politzer, *ibid.* **30**, 1346 (1973).
[2] L. N. Cooper, Phys. Rev. **104**, 1189 (1956).
[3] M. G. Alford, K. Rajagopal, and F. Wilczek, Phys. Lett. B **422**, 247 (1998).
[4] K. Rajagopal and F. Wilczek, arXiv:hep-ph/0011333; D. K. Hong, Acta Phys. Pol. B **32**, 1253 (2001); M. G. Alford, Annu. Rev. Nucl. Part. Sci. **51**, 131 (2001); G. Nardulli, Riv. Nuovo Cimento Soc. Ital. Fis. **25N3**, 1 (2002); T. Schafer, arXiv:hep-ph/0304281; D. H. Rischke, Prog. Part. Nucl. Phys. **52**, 197 (2004).
[5] Y. Nambu and G. Jona-Lasinio, Phys. Rev. **122**, 345 (1961); **124**, 246 (1961).
[6] T. Hatsuda and T. Kunihiro, Phys. Rep. **247**, 221 (1994); M. Buballa, Phys. Rep. **407**, 205 (2005).
[7] M. Huang, Int. J. Mod. Phys. E **14**, 675 (2005).
[8] S. Weinberg, Phys. Rev. D **56**, 2303 (1997).
[9] D. J. Gross and A. Neveu, Phys. Rev. D **10**, 3235 (1974).
[10] B. Rosenstein, B. J. Warr, and S. H. Park, Phys. Rep. **205**, 59 (1991).
[11] T. Inagaki, T. Kouno, and T. Muta, Int. J. Mod. Phys. A **10**, 2241 (1995); S. Kanemura, H.-T. Sato, Mod. Phys. Lett. A **10**, 1777 (1995); A. P. C. Malbouisson, J. M. C. Malbouisson, A. E. Santana, and J. C. da Silva, Int. J. Mod. Phys. A **20**, 4638 (2005); J. Feinberg and S. Hillel, J. Phys. A **39**, 6341 (2006); J.-L. Kneur, M. B. Pinto, and R. O. Ramos, Phys. Rev. D **74**, 125020 (2006); B. Charneski, A. F. Ferrari, and M. Gomes, J. Phys. A **40**, 3633 (2007).
[12] U. Wolff, Phys. Lett. B **157**, 303 (1985).
[13] K. G. Klimenko, Z. Phys. C **37**, 457 (1988).
[14] H. Kohyama, Phys. Rev. D **77**, 045016 (2008).
[15] A. Niegawa, Mod. Phys. Lett. A **23**, 933 (2008).
[16] P. C. Hohenberg, Phys. Rev. **158**, 383 (1967).
[17] N. D. Mermin and H. Wagner, Phys. Rev. Lett. **17**, 1133 (1966).
[18] J. Goldstone, A. Salam and S. Weinberg, Phys. Rev. **127**, 965 (1962).
[19] S. R. Coleman, Commun. Math. Phys. **31**, 259 (1973).
[20] T. W. Appelquist, M. Bowick, D. Karabali, and L. C. R. Wijewardhana, Phys. Rev. D **33**, 3704 (1986).
[21] D. Ebert, K. G. Klimenko, and H. Toki, Phys. Rev. D **64**, 014038 (2001).
[22] D. T. Son, Phys. Rev. D **59**, 094019 (1999); T. Schafer and F. Wilczek, Phys. Lett. B **450**, 325 (1999); N. J. Evans, S. D. H. Hsu, and M. Schwetz, Nucl. Phys. B **551**, 275 (1999).
[23] Y. Nambu, Phys. Rev. **117**, 648 (1960); L. P. Gorkov, JETP **7**, 993 (1958).
[24] M. L. Bellac, *Thermal Field Theory* (Cambridge University Press, Cambridge, England, 1996).